JACS
JOURNAL OF THE AMERICAN CHEMICAL SOCIETY
pubs.acs.org/JACS
Communication

Electrochemical Doping of Two-Dimensional Superatomic Materials

Shoushou He,[‡] Jessica Yu,[‡] William D. H. Stinson, Claire A. Looney, Saya Okuno, Andrew C. Crowther, Daniel V. Esposito, Michael L. Steigerwald,* Xavier Roy,* and Colin Nuckolls*

Cite This: *J. Am. Chem. Soc.* 2024, 146, 18861−18865
Read Online
ACCESS | Metrics & More | Article Recommendations | Supporting Information

ABSTRACT: We report an electrochemical method for doping two-dimensional (2D) superatomic semiconductor $Re_6Se_8Cl_2$ that significantly improves the material's electrical transport while retaining the in-plane and stacking structures. The electrochemical reduction induces the complete dissociation of chloride anions from the surface of each superatomic nanosheet. After the material is dehalogenated, we observe the electrical conductivity (σ) increases by two orders of magnitude while the 3D electron carrier density (n_{3D}) increases by three orders of magnitude. In addition, the thermal activation energy (E_a) and electron mobility (μ_e) decrease. We conclude that we have achieved effective electron-doping in 2D superatomic $Re_6Se_8Cl_2$, which significantly improves the electrical transport properties. Our work sets the foundation for electrochemically doping and tuning the transport properties of other 2D superatomic materials.

This manuscript describes a method to dope two-dimensional (2D) superatomic materials using electrochemistry to dramatically increase their electrical conductivity and carrier density. In contrast to atomic 2D materials, 2D superatomic materials are composed of atomically precise clusters that, akin to atoms, can be robust fundamental building units of solids.[1−3] The well-defined structures of 2D superatomic materials allow for the predictable modification of their surfaces and the potential for manipulating their properties.[4−6] Traditional methods to tune the electrical transport properties of semiconductors rely heavily on doping. For example, pristine silicon can be *n*- or *p*-doped by chemically replacing a small amount of silicon atoms with phosphorus or boron, respectively.[7−9] However, substituting one cluster for another is not achievable in superatomic solids. We thus need to develop a generalizable doping strategy to tune the electrical transport properties of 2D superatomic semiconductors so we can continue exploring them in next-generation nanoelectronics.[10,11] Electrochemical intercalation has been widely explored to dope traditional atomic van der Waals (vdW) materials with electrons for improving their electrical conductivity and increasing their carrier density.[12,13] Reductive doping has also been done on molecular clusters via chemical routes, such as by using Mashima's reagent.[14] Here, we harness the power of electrochemistry to induce a complete chemical transformation on the surface of a 2D superatomic material. We can use this method to dope 2D superatomic materials and tune their electrical transport properties. $Re_6Se_8Cl_2$ provides a platform to explore such experiments. It is a prototypical example of 2D vdW superatomic material that is composed of atomically precise Re_6Se_8 clusters, formed with Re_6 octahedra and Se on the octahedral faces (Figure 1).[15] The Re_6Se_8 clusters are linked covalently along the *a* and *b* crystallographic directions to form 2D layers, which stack to form the bulk vdW crystal. Each surface *trans*-Re atom is capped by a Cl atom, which we can selectively manipulate to modify the materials' properties.[16]

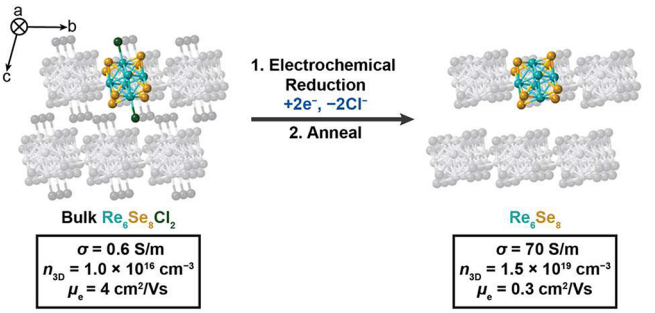

Figure 1. Doping induced by electrochemical Cl^- dissociation. The conductivities (σ), bulk carrier densities (n_{3D}), and electron mobilities (μ_e) at 300 K are shown.

Previous studies on $Re_6Se_8Cl_2$ have shown that superconductivity can arise after current annealing, but this harsh process can lead to irreversible damage to the 2D superatomic structure and the nature of the current annealed material is unclear.[17] Moreover, chemical substitution of the Cl atoms with a host of different surface moieties does not effectively result in doping and increased conductivity.[5] Here, we demonstrate complete removal of the Cl from $Re_6Se_8Cl_2$ single crystals by applying a small reducing potential, yielding Re_6Se_8. Unlike previous studies,[5,16] our electrochemical method cleaves all of the Re−Cl covalent bonds under mild

Received: May 6, 2024
Revised: June 28, 2024
Accepted: July 1, 2024
Published: July 3, 2024

https://doi.org/10.1021/jacs.4c06187
J. Am. Chem. Soc. 2024, 146, 18861−18865

reaction conditions within minutes, while the in-plane superatomic crystallinity and stacking are retained (Figure 1). Additionally, this treatment results in improved electrical transport properties in Re_6Se_8. We observe an increase in conductivity (σ) and electron carrier density (n_{3D}) by two and three orders of magnitude, respectively. Meanwhile, the thermal activation energy (E_a) and electron mobility (μ_e) decrease. These results indicate successful electron doping. Due to the simplicity of this method, we expect that it will be general and can be applied to other 2D superatomic materials.

We prepare $Re_6Se_8Cl_2$ single crystals via a chemical vapor transport method that has been adapted from a previous report.[16,18] For the electrochemistry on this material, we employ a three-electrode setup in 0.1 M KOH aqueous solution (Figure 2A). For the working electrode, we attach the $Re_6Se_8Cl_2$ single crystal to a fluorine-doped tin oxide (FTO) substrate with silver paint. A graphite rod and Ag/AgCl (3 M KCl) electrode are the counter (CE) and reference electrodes (RE), respectively. We can remove the Cl from the $Re_6Se_8Cl_2$ single crystal by performing cyclic voltammetry (CV) between 1.0 and −0.3 V vs the reversible hydrogen electrode (RHE) at 100 mV/s (Figures 2B inset and S1). We use energy-dispersive X-ray spectroscopy (EDX) to confirm complete Cl loss and the Re_6Se_8 composition (Figures S2−3 and Table S1). These results confirm that the electrochemical reduction induces fast Cl loss, resulting in the formation of Re_6Se_8. We identify the reduction as the peak spanning from 0 to 0.2 V vs RHE (Figure 2B inset). Based on this observation, we find that we can also completely remove the Cl from the material using chronoamperometry (CA) at −0.3 V vs RHE (Figure 2B), which is beyond the reduction peak in CV. Note that we observe no reduction of $Re_6Se_8Cl_2$ or loss of Cl at less reducing potentials. During the CA at −0.3 V vs RHE, the Cl removal from a $Re_6Se_8Cl_2$ single crystal reaches completion within 15 min when the current drops to the baseline level (vertical dashed line in Figure 2B). By integrating the shaded area in yellow, we obtain the number of electrons used to reduce a $Re_6Se_8Cl_2$ single crystal of known mass. The number of Cl atoms in the $Re_6Se_8Cl_2$ single crystal is consistent with the number of electrons in reduction, strongly suggesting that the reaction is a reduction and each chlorine is removed with one electron as Cl^- (see the Supporting Information for detail), while the remaining electron from each Re−Cl bond stays in the 2D superatomic framework. This is further supported by our electrical transport measurements discussed below. Thus, we have developed electrochemical reduction as a strategy for doping superatomic solids. Upon Cl^- dissociation, Re_6Se_8 flakes with thicknesses of ∼10−30 μm fall off from the $Re_6Se_8Cl_2$ crystal surface. We collect these flakes for device fabrication to probe the change in transport properties induced by electrochemical reduction.

We find when we electrochemically remove the chlorides, the electrical transport properties improve as a result of electron-doping. To test this, we fabricate electrical devices using Re_6Se_8 flakes as channel materials. We first dry the Re_6Se_8 flakes under vacuum at room temperature, and then

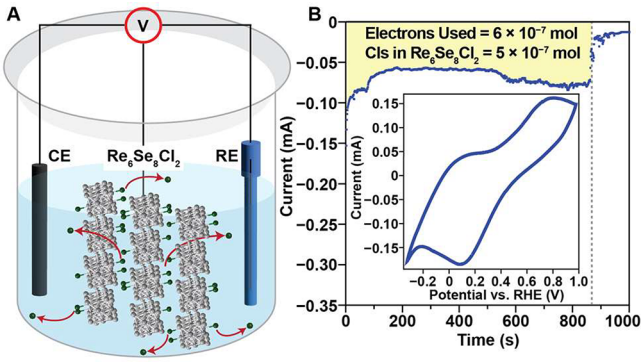

Figure 2. (A) Electrochemical reduction of $Re_6Se_8Cl_2$ for complete Cl^- removal. The Se and Re are shown in gray for clarity. (B) Chronoamperometry (CA) at −0.3 V vs RHE in 0.1 M KOH(aq) electrolyte solution for reducing $Re_6Se_8Cl_2$; the number of electrons used to reduce $Re_6Se_8Cl_2$ (obtained by integrating the area shaded in yellow) and the number of chlorines in the $Re_6Se_8Cl_2$ single crystal are shown. The dashed line marks the time at which the current drops to the baseline level, indicating the completion of reaction. A cyclic voltammogram (CV) in a typical protocol to remove Cl^- from $Re_6Se_8Cl_2$ is shown in the inset. CV is collected in 0.1 M KOH(aq) electrolyte solution at 100 mV/s scan rate.

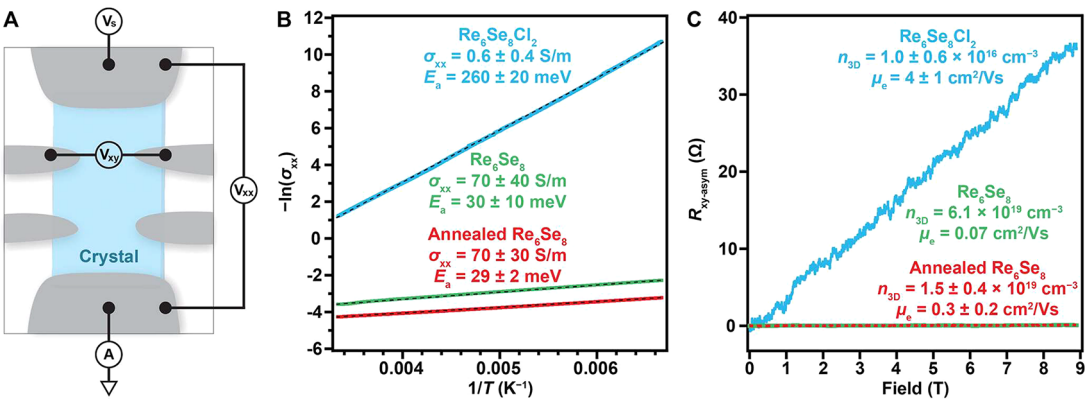

Figure 3. (A) A schematic representation of device configuration for longitudinal (R_{xx}) and Hall resistance (R_{xy}) measurements. (B) $-\ln(\sigma_{xx})$ versus $1/T$ Arrhenius plots, where σ_{xx} is the longitudinal conductivity and T is temperature. The linear fits are shown as black dashed lines. The conductivities (σ_{xx}) at 300 K and the activation energies (E_a) are shown. (C) Antisymmetrized Hall magnetoresistance ($R_{xy\text{-}asym}$) plots at 300 K. The Re_6Se_8 (green line) and its annealed solid (dashed red line) have similar $R_{xy\text{-}asym}$ slopes, giving overlapping plots. The bulk electron carrier densities (n_{3D}) and electron mobilities (μ_e) at 300 K are shown. The n_{3D} and μ_e for Re_6Se_8 is an average of two devices as we were unable to perform Hall measurements on the third device due to low electron mobility.

https://doi.org/10.1021/jacs.4c06187
J. Am. Chem. Soc. 2024, 146, 18861−18865

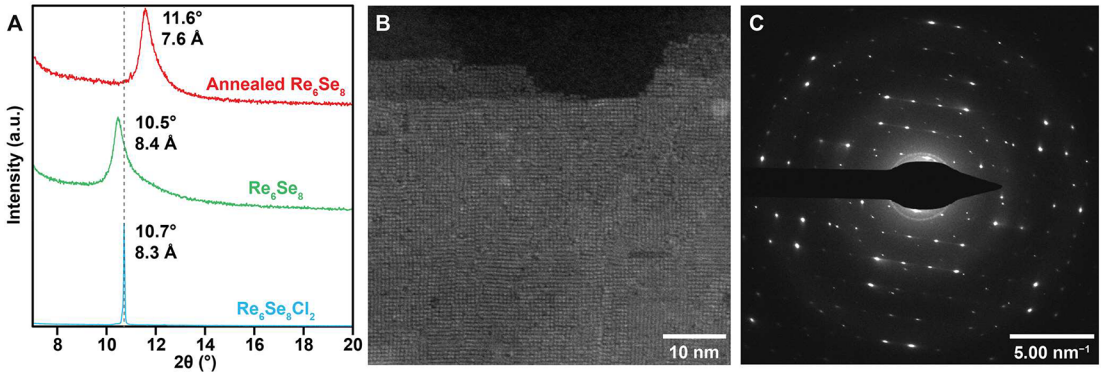

Figure 4. (A) PXRD patterns of a $Re_6Se_8Cl_2$ single crystal, Re_6Se_8, and annealed Re_6Se_8 between $2\theta = 7°$ and 20°. The change in (001) peak position is indicated by the dashed line. (B) HR-STEM image of a bilayer region of Re_6Se_8. (C) SAED pattern of a Re_6Se_8 multilayer.

adhere them with epoxy onto a borosilicate substrate. We make electrical contact to the flakes using silver paint. The contacts are arranged in a geometry, allowing for both longitudinal (R_{xx}) and Hall resistance (R_{xy}) measurements (Figures 3A and S4−6). We measure the electrical conductivity, activation energy, bulk carrier density, and electron mobility of both Re_6Se_8 and pristine $Re_6Se_8Cl_2$ (Figures 3B and C). For pristine $Re_6Se_8Cl_2$, the correlation between conductivity and temperature indicates a semiconductor-type behavior in which the conductivity increases with increasing temperature (Figure S7). We observe that the electrical conductivity of Re_6Se_8 (σ_{xx} = 70 ± 40 S/m) is two orders of magnitude higher than that of $Re_6Se_8Cl_2$ (σ_{xx} = 0.6 ± 0.4 S/m), while the thermally activated transport behavior persists in the measured temperature range of 50 to 300 K (Figures 3B and S7−8; Tables S2−3). Fitting to the Arrhenius equation $\ln(\sigma_{xx}) \propto \frac{E_a}{k_B T}$, where σ_{xx} is the longitudinal conductivity, E_a is the thermal activation energy, k_B is the Boltzmann constant, and T is the temperature, we obtain the activation energy and observe that it decreases by almost an order of magnitude (Figures 3B and S7−8; Tables S2−3). When we reduce $Re_6Se_8Cl_2$ and cleave the Re−Cl bonds, we anticipate the electrons doped into Re_6Se_8 will occupy the mid gap states (Figure 3B), thus reducing the activation energy from 260 ± 20 meV to 30 ± 10 meV. From the Hall effect measurements, we identify electrons as majority carriers in both $Re_6Se_8Cl_2$ and Re_6Se_8. The bulk electron carrier density (n_{3D}) increases by 6100 times from 1.0 ± 0.6 × 10^{16} cm^{-3} in $Re_6Se_8Cl_2$ to 6.1 × 10^{19} cm^{-3} in Re_6Se_8 (Figure 3C and Tables S2−3); this is consistent with electrons being injected into the material via electrochemical reduction. Note that we can control the electrochemical process to partially remove Cl^- from $Re_6Se_8Cl_2$. When we remove ∼75% of the Cl^-, the resulting conductivity (σ_{xx} at 300 K = 19 S/m) and activation energy (E_a = 50 meV) lie between those of $Re_6Se_8Cl_2$ and Re_6Se_8 (Table S4). Taken together, these transport results are indicative of electrons being doped into the material via electrochemical reduction.

Compared to $Re_6Se_8Cl_2$, Re_6Se_8 shows a decrease in electron mobility by a factor of 60 (Figure 3C and Tables S2−3). This could be explained by the structural imperfections in Re_6Se_8 created during or after the electrochemical process, including defects, changes in out-of-plane registry, and coordination of molecules on the surface of superatomic nanosheets. To remove some of these structural imperfections, we anneal the Re_6Se_8 flakes at 350 °C under vacuum for 24 h. The electrical conductivity of the annealed Re_6Se_8 (σ_{xx} at 300 K = 70 ± 30 S/m) is similar to that of Re_6Se_8 and is significantly higher than that of $Re_6Se_8Cl_2$ (Figure 3B). We observe the same trend in the activation energy and bulk electron density (Figures 3B and C). This shows that the annealing does not affect the electron-doping resulting from the electrochemical reduction of $Re_6Se_8Cl_2$. However, annealing enhances the electron mobility from 0.07 cm^2/Vs in Re_6Se_8 to 0.3 ± 0.2 cm^2/Vs in the annealed material (Figures 3C and S9; Table S5). The electron mobility of annealed Re_6Se_8 still remains an order of magnitude lower than that of $Re_6Se_8Cl_2$ due to the increase in carrier density and inability to remove all structural imperfections. Overall, our electrical transport measurements establish that the electrochemical reduction effectively dopes the superatomic $Re_6Se_8Cl_2$ with electrons. Since electrochemical Cl^- dissociation compromises the single crystallinity in $Re_6Se_8Cl_2$, these transport results only define the lower bound of what electrochemical doping can achieve.

To understand how the electrochemical doping affects the structure, we investigate the stacking structures using powder X-ray diffraction (PXRD) (Figures 4A and S10). The Re_6Se_8 exhibits a slightly larger interlayer spacing of 8.4 Å than does $Re_6Se_8Cl_2$. Compared to $Re_6Se_8Cl_2$ and Re_6Se_8, the annealed Re_6Se_8 exhibits a smaller interlayer spacing of 7.6 Å (Figure 4A). We further probe the in-plane superatomic structure using high-resolution scanning transmission electron microscopy (HR-STEM). To prepare the sample, we first exfoliate the Re_6Se_8 flakes by sonicating them in *N*-methylformamide (NMF) to produce a well-dispersed suspension of nanosheets, which we dropcast onto a TEM grid. HR-STEM reveals that the Cl^- removal from $Re_6Se_8Cl_2$ single crystals does not disrupt the 2D structure formed by covalently linked clusters (Figure 4B); we also confirm this with Raman spectroscopy since the Re−Se vibrational modes between 140 and 300 cm^{-1} persist (Figure S11). Furthermore, the selected area electron diffraction (SAED) of a Re_6Se_8 multilayer shows a pseudosquare lattice that is also present in $Re_6Se_8Cl_2$ (Figure 4C). The intercluster distance of the Re_6Se_8 nanosheet along the (100) and (010) is 6.5 Å, which is in good agreement with that of $Re_6Se_8Cl_2$ (6.6 Å). After annealing, the flakes do not exfoliate or suspend in NMF. As a result, we observe only bulk flakes and fragmented multilayers in the HR-STEM of annealed Re_6Se_8 (Figure S12). This observation is consistent with the PXRD results, which reveal that thermal annealing induces a decrease in interlayer spacing and thus tighter interactions. The intercluster distances in annealed Re_6Se_8 (6.4

https://doi.org/10.1021/jacs.4c06187
J. Am. Chem. Soc. 2024, 146, 18861−18865

and 6.2 Å; Figure S13) remain comparable with those of $Re_6Se_8Cl_2$. Overall, our HR-STEM measurements strongly suggest that the in-plane superatomic structure is maintained after electrochemistry and annealing.

We have little direct evidence concerning the intimate details of the chemical processes involved; however, we propose the following based on what can be experimentally observed. vdW attraction between the adjacent Cl-terminated sheets holds $Re_6Se_8Cl_2$ together; when we electrochemically reduce the material, chloride anions dissociate and the resulting Re_6Se_8 sheets spontaneously detach from the bulk crystal. Since PXRD shows an increase in the interlayer spacing when the chlorides leave, it is reasonable to postulate that something occupies the *trans*-Re sites. The most likely candidates are oxygen-based (water, hydroxyl, dioxygen, or some combination thereof) or hydrogen-based (Re−H). Upon annealing, the annealed Re_6Se_8 densifies along the stacking direction as indicated by PXRD, and it can no longer be exfoliated. We conclude from this that interlayer bonding of some sort has occurred: we suggest an O-based bridging layer, such as Re−O−Re. The interlayer spacing of 7.6 Å corresponds well with the Re−O−Re bond length in an oxo-bridged dimer of oxochalcohalide rhenium clusters and in a molecular compound reported in the literature.[19,20] While one might expect Fourier-transform infrared spectroscopy (FT-IR), Raman spectroscopy, and X-ray photoelectron spectroscopy (XPS) to provide evidence for these proposals, these experiments do not yield any useful information (Figures S11, S14, and S15). We conclude that the distribution of the surface species is not homogeneous enough for these methods to be conclusive.

In conclusion, we use electrochemistry to modify the surface of each constituent nanosheet in a superatomic $Re_6Se_8Cl_2$ single crystal. The material obtained via this method cannot be achieved by conventional solid-state chemistry techniques, demonstrating the power of postsynthetic modification in 2D superatomic materials. We can significantly enhance the electrical transport properties by doping the material with electrons through Cl^- dissociation driven by electrochemical reduction. Our work sets the foundation for electrochemically doping other vdW materials with labile halide surface ligands to enhance their electrical transport properties.

■ ASSOCIATED CONTENT

Supporting Information

The Supporting Information is available free of charge at https://pubs.acs.org/doi/10.1021/jacs.4c06187.

Materials, experimental methods, and characterization, including EDX, FT-IR, Raman, XPS, PXRD, HR-STEM, and transport measurements (PDF)

■ AUTHOR INFORMATION

Corresponding Authors

Colin Nuckolls − *Department of Chemistry, Columbia University, New York, New York 10027, United States;* orcid.org/0000-0002-0384-5493; Email: cn37@columbia.edu

Xavier Roy − *Department of Chemistry, Columbia University, New York, New York 10027, United States;* orcid.org/0000-0002-8850-0725; Email: xr2114@columbia.edu

Michael L. Steigerwald − *Department of Chemistry, Columbia University, New York, New York 10027, United States*; Email: mls2064@columbia.edu

Authors

Shoushou He − *Department of Chemistry, Columbia University, New York, New York 10027, United States;* orcid.org/0000-0001-5587-4854

Jessica Yu − *Department of Chemistry, Columbia University, New York, New York 10027, United States*

William D. H. Stinson − *Department of Chemical Engineering, Columbia University, New York, New York 10027, United States*

Claire A. Looney − *Department of Chemistry, Barnard College, New York, New York 10027, United States*

Saya Okuno − *Department of Chemistry, Columbia University, New York, New York 10027, United States*

Andrew C. Crowther − *Department of Chemistry, Barnard College, New York, New York 10027, United States;* orcid.org/0000-0003-2696-3211

Daniel V. Esposito − *Department of Chemical Engineering, Columbia University, New York, New York 10027, United States;* orcid.org/0000-0002-0550-801X

Complete contact information is available at: https://pubs.acs.org/10.1021/jacs.4c06187

Author Contributions

‡S.H. and J.Y. contributed equally.

Notes

The authors declare no competing financial interest.

■ ACKNOWLEDGMENTS

Research into the surface functionalization of 2D materials was supported by the NSF CAREER award DMR-1751949 (X.R.). Work on superatomic materials was supported by the NSF through the Columbia University Materials Research Science and Engineering Center (MRSEC) on Precision-Assembled Quantum Materials DMR-2011738 and the Air Force Office of Scientific Research award FA9550-22-1-0389 (X.R., C.N., M.L.S.). C.N. thanks Sheldon and Dorothea Buckler for their generous support. S.H. is a Postgraduate Scholar-Doctoral (PGS-D) supported by the National Sciences and Engineering Research Council of Canada (NSERC). The authors thank Dr. Tai-De Li from the City University of New York for conducting the XPS measurements. The authors thank Dr. Amirali Zangiabadi for his help with HR-STEM. The authors acknowledge the Columbia University Shared Materials Characterization Lab and the Electron Microscopy Lab.

■ REFERENCES

(1) Doud, E. A.; Voevodin, A.; Hochuli, T. J.; Champsaur, A. M.; Nuckolls, C.; Roy, X. Superatoms in materials science. *Nat. Rev. Mater.* **2020**, *5*, 371.

(2) Castleman, A. W.; Khanna, S. N. Clusters, superatoms, and building blocks of new materials. *J. Phys. Chem. C* **2009**, *113*, 2664.

(3) Jena, P.; Sun, Q. Super Atomic Clusters: Design Rules and Potential for Building Blocks of Materials. *Chem. Rev.* **2018**, *118*, 5755.

(4) Zhong, X.; Lee, K.; Meggiolaro, D.; Dismukes, A. H.; Choi, B.; Wang, F.; Nuckolls, C.; Paley, D. W.; Batail, P.; De Angelis, F.; Roy, X.; Zhu, X.-Y. $Mo_6S_3Br_6$: An Anisotropic 2D Superatomic Semiconductor. *Adv. Funct. Mater.* **2019**, *29*, 1902951.

(5) He, S.; Evans, A. M.; Meirzadeh, E.; Han, S. Y.; Russell, J. C.; Wiscons, R. A.; Bartholomew, A. K.; Reed, D. A.; Zangiabadi, A.;

Steigerwald, M. L.; Nuckolls, C.; Roy, X. Site-Selective Surface Modification of 2D Superatomic Re_6Se_8. *J. Am. Chem. Soc.* **2022**, *144*, 74.
(6) He, S.; Okuno, S.; Ng, F. W.; Pang, X.; Esposito, D. V.; Orchanian, N. M.; Steigerwald, M. L.; Roy, X.; Nuckolls, C. Functional Monolayers on a Superatomic Pegboard. *J. Am. Chem. Soc.* **2023**, *145*, 8314.
(7) Cui, Y.; Duan, X.; Hu, J.; Lieber, C. M. Doping and electrical transport in silicon nanowires. *J. Phys. Chem. B* **2000**, *104*, 5213.
(8) Arduca, E.; Perego, M. Doping of silicon nanocrystals. *Mater. Sci. Semicond. Process.* **2017**, *62*, 156.
(9) Spear, W. E.; Le Comber, P. G. Substitutional doping of amorphous silicon. *Solid State Commun.* **1975**, *17*, 1193.
(10) Di Paolo Emilio, M. *Microelectronics from Fundamentals to Applied Design*; Springer Press: 2016.
(11) Roy, X.; Lee, C. H.; Crowther, A. C.; Schenck, C. L.; Besara, T.; Lalancette, R. A.; Siegrist, T.; Stephens, P. W.; Brus, L. E.; Kim, P.; Steigerwald, M. L.; Nuckolls, C. Nanoscale Atoms in Solid-State Chemistry. *Science* **2013**, *341*, 157.
(12) Xiong, F.; Wang, H.; Liu, X.; Sun, J.; Brongersma, M.; Pop, E.; Cui, Y. Li Intercalation in MoS_2: In Situ Observation of Its Dynamics and Tuning Optical and Electrical Properties. *Nano Lett.* **2015**, *15*, 6777.
(13) Martinez, E. Y.; Zhu, K.; Li, C. W. Reversible Electron Doping of Layered Metal Hydroxide Nanoplates (M = Co, Ni) Using *n*-Butyllithium. *Nano Lett.* **2020**, *20*, 7580.
(14) Chakraborty, S.; Matson, E. M. Reductive silylation of polyoxovanadate surfaces using Mashima's reagent. *Inorg. Chem. Front.* **2021**, *8*, 4507.
(15) Zhong, X.; Lee, K.; Choi, B.; Meggiolaro, D.; Liu, F.; Nuckolls, C.; Pasupathy, A.; De Angelis, F.; Batail, P.; Roy, X.; Zhu, X. Superatomic Two-Dimensional Semiconductor. *Nano Lett.* **2018**, *18*, 1483−1488.
(16) Choi, B.; Lee, K.; Voevodin, A.; Wang, J.; Steigerwald, M. L.; Batail, P.; Zhu, X.; Roy, X. Two-Dimensional Hierarchical Semiconductor with Addressable Surfaces. *J. Am. Chem. Soc.* **2018**, *140*, 9369.
(17) Telford, E. J.; Russell, J. C.; Swann, J. R.; Fowler, B.; Wang, X.; Lee, K.; Zangiabadi, A.; Watanabe, K.; Taniguchi, T.; Nuckolls, C.; Batail, P.; Zhu, X.; Malen, J. A.; Dean, C. R.; Roy, X. Doping-Induced Superconductivity in the van der Waals Superatomic Crystal $Re_6Se_8Cl_2$. *Nano Lett.* **2020**, *20*, 1718.
(18) Leduc, L.; Perrin, A.; Sergent, M. Structure du dichlorure et octaséléniure d'hexarhénium, $Re_6Se_8Cl_2$: composé bidimensionnel à clusters octaédriques Re_6. *Acta Crystallogr. Sect. C* **1983**, *39*, 1503.
(19) Lock, C. J. L.; Turner, G. Studies of the rhenium-oxygen bond. II. The crystal and molecular structure of μ-oxobis(cis-dichloro-cis-di(pyridine)-trans-oxorhenium(V)), $ORe(C_5H_5N)_2Cl_2ORe(C_5H_5N)_2Cl_2O$. *Can. J. Chem.* **1978**, *56*, 179.
(20) Simon, F.; Boubekeur, K.; Gabriel, J.-C. P.; Batail, P. $[NBu^n_4]_4[(Re_6S_5OCl_7)_2O]$, an oxo-bridged siamese twin cluster of two hexanuclear oxochalcohalide rhenium clusters. *Chem. Commun.* **1998**, 845.

https://doi.org/10.1021/jacs.4c06187
J. Am. Chem. Soc. 2024, 146, 18861−18865